Inorg. Chem. **2007**, *46*, 8362–8371

Inorganic Chemistry
Article

Iron Chelation Equilibria, Redox, and Siderophore Activity of a Saccharide Platform Ferrichrome Analogue

Suraj Dhungana,[†] James M. Harrington,[†] Peter Gebhardt,[‡] Ute Möllmann,[‡] and Alvin L. Crumbliss*[,†]

Department of Chemistry, Duke University, Box 90346 Durham, North Carolina 27708-0346,
and Leibniz Institute for Natural Product Research and Infection Biology, Hans Knöll-Institut,
Jena, Germany

Received January 29, 2007

A complete characterization of the aqueous solution Fe(III) and Fe(II) coordination chemistry of a saccharide-based ferrichrome analogue, 1-*O*-methyl-2,3,6-tris-*O*-[4-(*N*-hydroxy-*N*-ethylcarbamoyl)-*n*-butyryl]-α-D-glucopyranoside ($H_3L_N^{236}$), is reported including relevant thermodynamic parameters and growth promotion activity with respect to both Gram-negative and Gram-positive bacterial strains. The saccharide platform is an attractive backbone for the design and synthesis of ferrichrome analogues because of its improved water solubility and hydrogen-bonding capabilities, which can potentially provide favorable receptor recognition and biological activity. The ligand deprotonation constants (pK_a values), iron complex ($Fe^{III}(L_N^{236})$ and $Fe^{II}(L_N^{236})^{1-}$) protonation constants ($K_{FeHxL-236-N}$), overall Fe(III) and Fe(II) chelation constants (β_{110}), and aqueous solution speciation were determined by spectrophotometric and potentiometric titrations, EDTA competition equilibria, and cyclic voltammetry. Log $\beta^{III}{}_{110} =$ 31.16 and pFe = 26.1 for $Fe^{III}(L_N^{236})$ suggests a high affinity for Fe(III), which is comparable to or greater than ferrichrome and other ferrichrome analogues. The $E_{1/2}$ for the $Fe^{III}(L_N^{236})/Fe^{II}(L_N^{236})^{1-}$ couple was determined to be –454 mV (vs NHE) from quasi-reversible cyclic voltammograms at pH 9. Below pH 6.5, the $E_{1/2}$ shifts to more positive values and the pH-dependent $E_{1/2}$ profile was used to determine the $Fe^{II}(L_N^{236})^{1-}$ protonation constants and overall stability constant log $\beta^{II}{}_{110} = 11.1$. A comparative analysis of similar data for an Fe(III) complex of a structural isomer of this exocyclic saccharide chelator ($H_3L_R^{234}$), including strain energy calculations, allows us to analyze the relative effects of the pendant arm position and hydroxamate moiety orientation (normal vs retro) on overall complex stability. A correlation between siderophore activity and iron coordination chemistry of these saccharide–hydroxamate chelators is made.

Introduction

The biological importance of iron is monumental, as it is essential for the growth and survival of almost all living organisms. Iron is the most abundant transition metal in the biosphere, and yet its bioavailability is severely limited by the formation of insoluble iron hydroxides.[1] In aqueous-aerobic conditions and neutral pH, the total concentration of soluble iron ($Fe_{(aq)}{}^{3+} + Fe(OH)_{(aq)}{}^{2+} + Fe(OH)_{2(aq)}{}^{+}$) is as low as 10^{-10} M.[2–4] This can be increased by the presence of chelating agents. Microorganisms that acquire iron directly from the environment produce iron-specific chelators called siderophores under iron-limiting conditions. Siderophores are low-molecular-weight organic molecules that are designed to selectively chelate Fe^{3+} in the presence of other environmentally prevalent metal ions. Bacterial siderophores normally express this selectivity through a high Fe^{3+} binding constant on the order of log $\beta > 30$, although plant siderophores often have much lower affinity constants. The ability of a microbe to efficiently acquire iron from the environment determines its growth and survival, and for pathogenic microbes, the efficiency of iron acquisition has proven to be an important virulence factor.[2,5–15]

---

* To whom correspondence should be addressed. E-mail: alc@chem.duke.edu. Fax: (919) 660-1605.

[†] Duke University.

[‡] Hans Knöll-Institut.

(1) Crichton, R. R. *Inorganic Biochemistry of Iron Metabolism: From Molecular Mechanism to Clinical Consequences*, 2nd ed.; Wiley: New York, 2001.
(2) Boukhalfa, H.; Crumbliss, A. L. *BioMetals* **2002**, *15*, 325–339.
(3) Chipperfield, J. R.; Ratledge, C. *BioMetals* **2000**, *13*, 165–168.
(4) Dhungana, S.; Crumbliss, A. L. *Geomicrobiol. J.* **2005**, *22*, 87–98.
(5) Albrecht-Gary, A.-M.; Crumbliss, A. L. *Metal Ions in Biological Systems*; Sigel, A., Sigel, H., Eds.; Marcel Dekker: New York, 1998; Vol. 35, pp 239–328.

10.1021/ic070158l CCC: $37.00

The iron release mechanism from highly stable iron−siderophore complexes still remains a topic of much debate; however, a major iron release pathway is believed to involve reduction of Fe^{3+} to Fe^{2+} and its subsequent transfer to various acceptor molecules within the cell membrane and/or cell interior.[2,4,12] Other mechanisms involving ligand exchange, hydrolysis of the siderophore ligand, and/or protonation of the iron−siderophore complex are also believed to be operative, depending on the microbial/siderophore uptake system.[2,5,13,16]

Synthetic siderophore mimics play an important role in our understanding of how natural siderophores function and in the development of new therapeutic agents.[17−20] Several factors are important in the design of siderophore mimics with high specificity for Fe(III), and these include donor groups, denticity, chelate ring size, architecture, hydrophobicity/hydrophilicity, and stability. Hexadentate chelators generally provide more-stable and less-labile iron(III) chelates, necessary characteristics for siderophores. Donor groups for iron chelation in siderophores usually include either hydroxamates or catechols,[5,6,9,13,21] but occasionally, siderophores with other donor groups have been identified, including α-hydroxy carboxylic acid[5,13] and β-hydroxyhistidine.[22−25] Siderophore architecture includes linear, tripodal, endocyclic, and exocyclic structures.[6,26] The desferrichromes are a family of exocyclic trihydroxamate fungal siderophores which serve as a natural prototype for the synthetic mimics described here. The architecture and hydrophilic/hydrophobic properties of siderophores and siderophore mimics are important in determining their efficacy. Enzymatic C-glucosylation of natural siderophore scaffolds has recently been described.[27,28] This modification results in reducing scaffold hydrophobicity[29] and in the case of enterobactin (e.g., salmochelin S4) hinders serum sequestration of the ferri-siderophore by siderocalin as a pathogen defense mechanism.[30]

Exocyclic and tripodal siderophore mimics have been successfully built around tertiary amine,[31] benzene,[32] and tetrahedral carbon as the backbone.[33,34] Recently we have explored using a cyclic saccharide platform on which to synthesize exocyclic tris catechol and hydroxamic acid chelators that have shown early promise as siderophore mimics. Thermodynamically, these synthetic analogues have Fe(III) chelation capabilities that are comparable if not greater than that of their natural counterparts.[35,36] Biologically, they are highly promising synthetic analogues, as in vivo studies show significant siderophore activity[37−39] indicating favorable cell receptor recognition and cellular uptake. These results indicate that the carbohydrate scaffold is a biologically viable backbone for exocyclic siderophore analogues. The synthetic versatility of carbohydrate chemistry, along with previously reported thermodynamic and biological properties, provides evidence that a series of saccharide platform chelators can be designed and studied to understand subtle and still-unexplored aspects of siderophore-mediated iron transport.

A synthetic analogue of desferrichrome, $H_3L_N^{236}$ (Figure 1), has been constructed on a methyl α-D-glucopyranoside scaffold with three asymmetric hydroxamic acid moieties attached to the saccharide unit: 1-*O*-methyl-2,3,6-tris-*O*-[4-(*N*-hydroxy-*N*-ethylcarbamoyl)-*n*-butyryl]-α-D-glucopyranoside. Earlier, a related desferrichrome model, $H_3L_R^{234}$ (Figure 1),[40] was synthesized[38] and characterized for its Fe(III) coordination properties.[36] The two saccharide platform trihydroxamate chelators, $H_3L_N^{236}$ and $H_3L_R^{234}$, differ in two

---

(6) Crumbliss, A. L. *Handbook of Microbial Iron Chelates*; Winkelmann, G., Ed.; CRC Press: Boca Raton, FL, 1991; pp 177−233.
(7) Matzanke, B. F.; Müller-Matzanke, G.; Raymond, K. N. *Iron Carriers and Iron Proteins*; Loehr, T. M., Ed.; VCH Publishers: New York, 1989; Vol. 5, pp 3−121.
(8) Neilands, J. B. *J. Biol. Chem.* **1995**, *270*, 26723−26726.
(9) Raymond, K. N.; Telford, J. R. *NATO ASI Series C, Mathematical and Physical Sciences*; Kessissoglous, D. P., Ed.; Kluwer Academic Publishers: Dordrecht, The Netherlands, 1995; Vol. 459, pp 25−37.
(10) Raymond, K. N.; Dertz, E. A. *Iron Transport in Bacteria*; Crosa, J. H., Mey, A. R., Payne, S. M., Eds.; American Society for Microbiology: Washington, DC, 2004; pp 3−17.
(11) Winkelmann, G. *Handbook of Microbial Iron Chelates*; CRC Press: Boca Raton, FL, 1991.
(12) Ratledge, C.; Dover, L. G. *Annu. Rev. Microbiol.* **2000**, *54*, 881−941.
(13) Stintzi, A.; Raymond, K. N. *Molecular and Cellular Iron Transport*; Templeton, D. M., Ed.; Marcel Dekker, Inc.: New York, 2002; pp 273−320.
(14) Philpott, C. C. *Biochim. Biophys. Acta* **2006**, *1763*, 636−645.
(15) Grass, G. *BioMetals* **2006**, *19*, 159−172.
(16) Raymond, K. N.; Dertz, E. A.; Kim, S. S. *Proc. Nat. Acad. Sci.* **2003**, *100*, 3584−3588.
(17) Richardson, D. R. *Crit. Rev. Oncol./Hemotol.* **2002**, *42*, 267−281.
(18) Liu, Z. D.; Hider, R. C. *Coord. Chem Rev.* **2002**, *232*, 151−171.
(19) Hershko, C. *Rev. Clin. Exp. Hematol.* **2000**, *4*, 337.
(20) Miller, M. J.; Darwish, I.; Ghosh, A.; Ghosh, M.; Hansel, J.; Hu, J.; Niu, C.; Ritter, A.; Scheidt, K.; Suling, C.; Sun, S.; Zhang, D.; Budde, A.; DeClercq, E.; Leong, S.; Malouin, F.; Moellmann, U. *Anti-Infectives: Recent Advances in Chemistry and Structure-Activity Relationships*; Bentley, P. H., O'Hanlon, P. J., Eds.; Royal Society of Chemistry: Cambridge, UK, 1997; pp 116−138.
(21) Meyer, M. T.-K., W. *Recent Res. Devel. Phys. Chem.* **2004**, *7*, 127−149.
(22) Sharman, G. J.; Williams, D. H.; Ewing, D. F.; Ratledge, C. *Chem. Biol.* **1995**, *2*, 553−561.
(23) Dong, L.; Miller, M. J. *J. Org. Chem.* **2002**, *67*, 4759−4770.
(24) Dhungana, S.; Miller, M. J.; Dong, L.; Ratledge, C.; Crumbliss, A. L. *J. Am. Chem. Soc.* **2003**, *125*, 7654−7663.
(25) Hancock, D. K.; Coxon, B.; Wang, S. Y.; White, E. V.; Reeder, D. J.; Bellama, J. M. *J. Chem. Soc., Chem. Commun.* **1993**, 468−469.
(26) Dertz, E. A.; Raymond, K. N. *Comprehensive Coordination Chemistry II*; McCleverty, J., Meyer, T. J., Eds.; Pergamon: Oxford, 2003; Vol. 8, pp 141−168.
(27) Hantke, K.; Nicholson, G. D.; Rabsch, W.; Winkelmann, G. *Proc. Natl. Acad. Sci U.S.A.* **2003**, *100*, 3677−3682.
(28) Bister, B.; Bischoff, D.; Nicholson, G. J.; Valdebenito, M.; Schneider, K.; Winkelmann, G.; Hantke, K.; Sassmuth, R. D. *BioMetals* **2004**, *17*, 471−481.
(29) Luo, M.; Lin, H.; Fischbach, M. A.; Liu, D. R.; Walsh, C. T.; Groves, J. T. *Chem. Biol.* **2006**, *1*, 29−32.
(30) Abergel, R. J.; Moore, E. G.; Strong, R. K.; Raymond, K. N. *J. Am Chem Soc.* **2006**, *128*, 10998−10999.
(31) Ng, C. Y.; Rodgers, S. J.; Raymond, K. N. *Inorg. Chem.* **1989**, *28*, 2062−2066.
(32) Yoshida, I.; Murase, I.; Motekaitis, R. J.; Martell, A. E. *Can. J. Chem.* **1983**, *61*, 2740−2744.
(33) Meijler, M. M.; Arad-Yellin, R.; Cabantchik, Z. I.; Shanzer, A. *J. Am. Chem. Soc.* **2002**, *124*, 12666−12667.
(34) Weizman, H.; Ardon, O.; Mester, B.; Libman, J.; Dwir, O.; Hadar, Y.; Chen, Y.; Shanzer, A. *J. Am. Chem. Soc.* **1996**, *118*, 12368−12375.
(35) Dhungana, S.; Heggemann, S.; Heinisch, L.; Moellmann, U.; Boukhalfa, H.; Crumbliss, A. L. *Inorg. Chem.* **2001**, *40*, 7079−7086.
(36) Dhungana, S.; Heggemann, S.; Gebhardt, P.; Moellmann, U.; Crumbliss, A. L. *Inorg. Chem.* **2003**, *42*, 42−50.
(37) Heggemann, S.; Schnabelrauch, M.; Klemm, D.; Möllmann, U.; Reissbrodt, R.; Heinisch, L. *BioMetals* **2001**, *14*, 1.
(38) Heggemann, S.; Möllmann, U.; Gebhardt, P.; Heinisch, L. *BioMetals* **2003**, *16*, 539−551.
(39) Gebhardt, P.; Crumbliss, A. L.; Miller, M. J.; Moellman, U. *BioMetals* **2007**, http://dx.doi.org/10.1007/s10534-007-9091-x.

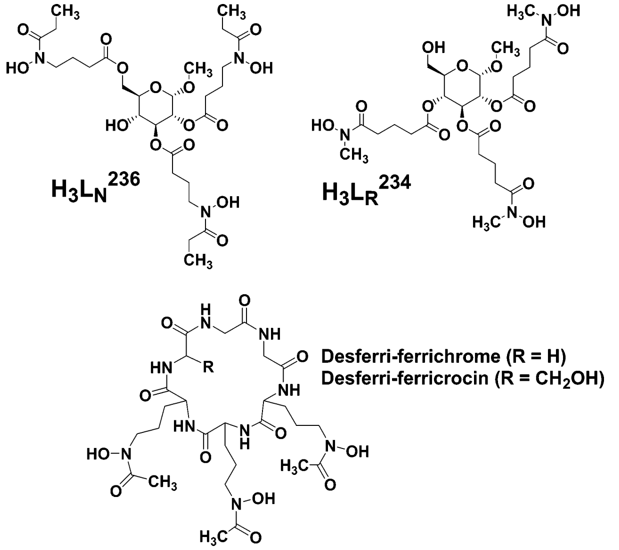

Figure 1. Desferrichrome and desferricrocin, naturally occurring exocyclic siderophores with hydroxamate functional groups, and two synthetic desferrichrome mimics with a saccharide backbone: 1-*O*-methyl-2,3,6-tris-*O*-[4-(*N*-hydroxy-*N*-ethylcarbamoyl)-*n*-butyryl]-α-D-glucopyranoside ($H_3L_N{}^{236}$) and the retrohydroxamate ($H_3L_R{}^{234}$).

respects: (1) $H_3L_N{}^{236}$ has a normal-hydroxamate geometry and $H_3L_R{}^{234}$ is a retrohydroxamate siderophore mimic (siderophore analogue in which the position of the hydroxamate nitrogen and carbon are interchanged relative to their position in the natural siderophore); (2) the equal-length pendant arms are attached to the saccharide backbone at different positions (2,3,4 vs 2,3,6). These two features allow for a comparative structure−property analysis. A small structural variation, like the normal-hydroxamate and the retro-hydroxamate, and 2,3,4 vs 2,3,6 exocyclic arm attachment, may have significant implications in a chelator's ability to bind Fe(III) and in the receptor recognition process. An investigation of synthetic analogues such as these allows us to investigate small structural changes on siderophores in order to understand and unravel the mechanistic intricacies of a highly fine-tuned iron acquisition and transport system that is ubiquitous among almost all microbes. Understanding the detailed functioning of such subtle structural differences is of significant interest, as this information can be used to design siderophores as penetration vectors for antibiotics or other biological applications involving Fe(III) uptake and metabolism.[20,41] This communication describes the detailed aqueous solution characterization of the Fe(III) and Fe(II) coordination properties of $H_3L_N{}^{236}$ and the corresponding comparison with $H_3L_R{}^{234}$, a retro-hydroxamate analogue with a shift in exocyclic arm placement (Figure 1). Also included are biological activity data which utilize wild-type and mutant Gram-negative and Gram-positive bacterial strains to explore what transport modes may be operative for these two siderophore mimics.

Experimental Section

Materials. All solutions were prepared in deionized water. All pH measurements were made using an Orion 230 A+ pH/ion meter equipped with an Orion ROSS pH electrode filled with 3 M NaCl solution. The pH of all solutions was adjusted with NaOH or $HClO_4$, accordingly. A stock solution of 2 M $NaClO_4$ was prepared from solid sodium perchlorate hydrate (Aldrich, 99+%) and standardized by passage through a Dowex 50 W-X8 strong acid cation-exchange column in H^+ form. The acid displaced from the column was titrated with standard NaOH solution to the phenolphthalein end point. A 2 M $HClO_4$ stock solution was prepared from concentrated perchloric acid (Fisher, 70%) and standardized by titration with standard NaOH solution to the phenolphthalein end point. An iron(III) perchlorate stock solution (0.1 M) was prepared from recrystallized $Fe(ClO_4)_3$ (Aldrich), standardized spectrophotometrically in strong acid[42] and titrimetrically by reduction with Sn(II) and titrated with the primary standard potassium dichromate.[43] Carbonate-free NaOH was prepared by diluting 1 M NaOH with deionized water purged with Ar for 45 min and standardized by titration with standard 0.2 M HCl to the phenolphthalein end point.

The synthesis and characterization of 1-*O*-methyl-2,3,6-tris-*O*-[4-(*N*-hydroxy-*N*-ethylcarbamoyl)-*n*-butyryl]-α-D-glucopyranoside ($H_3L_N{}^{236}$) are described elsewhere.[39] The tris(hydroxamate)iron(III) complex ($Fe^{III}(L_N{}^{236})$) was formed by adding 1 equiv of acidic $Fe_{aq}{}^{3+}$ to an aqueous solution of the ligand and slowly increasing the pH to 9, with constant stirring over the course of 45−60 min.

Methods. Potentiometric Measurements. All solutions were purged with Ar prior to titration. Samples (10 mL) were placed in a double-walled titration cell maintained at 25.00 ± 0.05 °C. A Titronic 96 standard burette was used to carry out conventional potentiometric titration experiments. Glass electrode calibration is described in the Supporting Information.[48] After each addition of standardized NaOH, UV−vis spectra were recorded using a Cary 100 spectrophotometer. Potentiometric and spectrophotometric data were analyzed simultaneously using HYPERQUAD,[44] as it allows for potentiometric and/or spectrophotometric data and the simultaneous treatment of multiple titration curves.

Spectrophotometric Measurements. Two separate and independent spectrophotometric titrations were carried out in the mid-pH range and low-pH range. UV−vis spectra of the iron complexes as a function of pH were obtained from a single stock solution using a Cary 100 spectrophotometer. The stock solution was divided into different aliquots, and each aliquot was separately used for a spectrophotometric titration. Titrations were carried out in both low-to-high-pH and high-to-low-pH directions, using a different aliquot of iron complex. After each adjustment of pH using a known

---

(40) In our previous paper, ref 36, this chelator was referred to as simply as H_3L. Here we refer to this chelator as $H_3L_R{}^{234}$ to reflect the exocyclic retro-hydroxamate-containing arms connected to the saccharide ring at the 2, 3, and 4 positions. This is in contrast to the chelator reported here which is designated as $H_3L_N{}^{236}$ to reflect the exocyclic normal-hydroxamate-containing arms connected to the saccharide ring at the 2, 3, and 6 positions. The structures of $H_3L_N{}^{236}$ and $H_3L_R{}^{234}$ are shown in Figure 1.

(41) Kalinowski, D. S.; Richardson, D. R. *Pharm. Rev.* **2005**, *57*, 547−583.

(42) Bastian, R.; Weberling, R.; Palilla, F. *Anal. Chem.* **1956**, *28*, 459−462.

(43) Vogel, A. I. *Quantitative Inorganic Analysis Including Elementary Instrumental Analysis*, 3rd ed.; Longmans, Green and Co., Ltd.: London, 1968.

(44) Gans, P.; Sabatini, A.; Vacca, A. *Talanta* **1996**, *43*, 1739−1753.

(45) Binstead, R. A.; Jung, B.; Zuberbühler, A. D. *SPECFIT/32 Global Analysis System*, 3.0; Spectrum Software Associates: Marlborough, MA, 2000.

(46) Martell, A. E.; Smith, R. M. *Critical Stability Constants*; Plenum Press: New York, 2001; Vol. 1.

(47) Wavefunction, Inc., 18401 Von Karman Avenue, Suite 370, Irvine, CA 92612.

(48) Supporting Information access may be found at the end of the manuscript.

Table 1. Ligand pK_a Values for $H_3L_N{}^{236}$ and $H_3L_R{}^{234}$ and Relevant Natural Siderophores

pK_{an}[a]	$H_3L_N{}^{236}$ [b]	$H_3L_R{}^{234}$ [c]	desferrichrome[d]	desferricrocin[e]
$n = 1$	8.87 ± 0.02	8.67 ± 0.03	8.11	8.14
$n = 2$	9.55 ± 0.01	9.31 ± 0.01	9.00	9.01
$n = 3$	9.99 ± 0.02	9.94 ± 0.01	9.83	9.92

[a] Defined by eq 1. Uncertainties listed were determined on the basis of the standard deviation and include estimated experimental error. [b] This work; conditions: $T = 298$ K and $\mu = 0.10$ M $NaClO_4$. [c] Reference 36. [d] Reference 55. [e] Reference 56.

Table 2. Protonation Constants for Iron(III) and Iron(II) Complexes of $H_3L_N{}^{236}$ and $H_3L_R{}^{234}$

	$H_3L_N{}^{236}$ [a]		$H_3L_R{}^{234}$ [b]	
	Fe(III)[c]	Fe(II)[d]	Fe(III)[c]	Fe(II)[d]
log K_{FeHL}	4.06 ± 0.02[e]	5.6 ± 0.1[g]	4.69 ± 0.05	6.6 ± 0.1
(pK_3)	4.08 ± 0.01[f]		4.2 ± 0.2	
log K_{H2L}	1.71 ± 0.02[e]	4.6 ± 0.2[g]	2.41 ± 0.10	5.1 ± 0.2
(pK_2)	1.72 ± 0.12[f]			
log K_{FeH3L}	0.66 ± 0.21[e]	3.5 ± 0.4[g]	0.61 ± 0.22	4.0 ± 0.2
(pK_1)	0.88 ± 0.11[f]			

[a] Conditions: $T = 298$ K and $\mu = 0.10$ M $NaClO_4$. Uncertainties listed were determined on the basis of the standard deviation and include estimated experimental error. [b] Reference 36. [c] As defined by eqs 3 and 4. [d] As defined by eqs 10, 11, and 12. [e] From HYPERQUAD[44] analysis. [f] From SPECFIT/32[45] analysis. [g] Calculated from electrochemical data in Figure 6 using eq 13.

Table 3. Fe−Siderophore Complex Thermodynamic Parameters

	log β_{110}[a]				
ligand	Fe(III)	Fe(II)	pFe[b] (mV)	$E_{1/2}$ vs NHE	ref
$H_3L_N{}^{236}$	31.14 ± 0.01[c] 31.16 ± 0.04[d] 31.1 ± 0.2[e]	11.1[f]	26.1	−454	this work
$H_3L_R{}^{234}$	31.86 ± 0.11	12.1	27.1	−436	36
desferrichrome	29.07	9.9	25.2	−400	55, 64
desferricrocin	30.4	11.6	26.5	−412	56
desferrioxamine B	30.60	10.3	26.6	−468	57, 65, 66,67

[a] Defined as $\beta_{110} = [FeL]/[Fe][L]$ for $Fe + L \rightleftharpoons FeL$ (charges omitted for clarity). Uncertainties listed were determined on the basis of the standard deviation and include estimated experimental error. [b] $-\log [Fe^{3+}]$ at $[Fe(III)]_{tot} = 10^{-6}$ M, $[ligand]_{tot} = 10^{-5}$ M, and pH = 7.4. [c] From SPECFIT/32[45] analysis using data from spectrophotometric titrations. [d] From HYPERQUAD[44] analysis using data from potentiometric and spectrophotometric titration. [e] EDTA competition experiments as defined in eqs 7 and 8. [f] Calculated from eq 9 using $E_{aquo} = +732$mV, consistent with previous work from this laboratory.[67]

volume of standardized acid or base, the solution was allowed to equilibrate for 30 min and its visible spectrum was recorded. Corrections were made for dilution due to the addition of acid and base; data were analyzed using SPECFIT/32[45] software. Since the volume of standardized strong acid or strong base added during the titration was recorded, HYPERQUAD[44] software was also used for the data analysis and the simultaneous treatment of multiple titration curves. SPECFIT/32[45] and HYPERQUAD[44] produced values for stability and protonation constants in agreement within experimental error, demonstrating that our results are independent of software data analysis methods. Hyperquad-determined values were used exclusively for pFe and β_{110} calculations for internal consistency, as Hyperquad was used to analyze ligand pK_a data needed to compute these values.

The calculated uncertainties for pK_a, log K, and log β listed in Tables 1, 2 and 3 were determined on the basis of the standard deviation and include estimated experimental error.

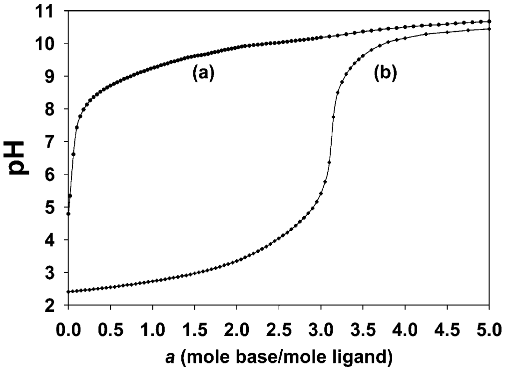

Figure 2. Potentiometric titration curves: (a) 1.1×10^{-4} M $H_3L_N{}^{236}$; (b) $H_3L_N{}^{236}$ and Fe^{3+}, 1:1, 5.0×10^{-4} M. Conditions: $T = 298$ K and $\mu = 0.10$ M $NaClO_4$.

Competition Equilibria with EDTA. Spectrophotometric experiments involving Fe(III) competition equilibria with $H_3L_N{}^{236}$ and EDTA were carried out over a pH range. The stock solution of $Fe^{III}-H_3L_N{}^{236}$ was divided into 16 different aliquots. Each aliquot (3 mL) was allowed to equilibrate with a fixed EDTA concentration at various pH values (pH 6.2−9.0, adjusted using strong acid/base to minimize the change in volume) for 1 week at 25 °C. No further change in the spectral profile indicated that the system had reached equilibrium. The equilibrium solutions contained 2.7×10^{-4} M Fe(III), 2.7×10^{-4} M $H_3L_N{}^{236}$, and 5.0×10^{-3} M EDTA. At the end of 1 week, UV−vis spectra and pH were recorded. Under equilibrium conditions at various pH, there were measurable amounts of reactants and products ($Fe^{III}-H_3L_N{}^{236}$, Fe^{III}−EDTA, $H_3L_N{}^{236}$, and EDTA) present in solution. These competition equilibrium data were refined to obtain the overall Fe(III)-binding constant (log $\beta^{III}{}_{110}$) for $H_3L_N{}^{236}$ using SPECFIT/32 software with a model involving two ligands and a metal.[45] The protonation constants and Fe(III) formation constants for EDTA[46] and the protonation constants for $H_3L_N{}^{236}$ were used as fixed parameters during data analysis.

Electrochemistry. Cyclic voltammograms of $Fe^{III}(L_N{}^{236})$ in aqueous 0.1 M $NaClO_4$ under Ar at room temperature were obtained using an EG&G Princeton Applied Research Potentiostat Model 263. Voltammograms were recorded using PowerCV software at a scan rate of 20 mV/s, with a HDME working electrode, Ag/AgCl (KCl saturated) reference electrode and platinum wire auxiliary electrode. Potentials referenced to Ag/AgCl (KCl saturated) were converted relative to NHE by adding 197 mV. The pH of the solution was adjusted using 1 M NaOH and 2 M $HClO_4$ to minimize the volume change. At low pH, the cyclic voltammogram becomes irreversible; the $E_{1/2}$ values at these pH's were estimated by assuming a peak-to-peak separation of 90 mV, as seen in the quasi-reversible case at higher pH.

Strain Energy Calculations. Strain energy calculations were performed using Spartan '02 by Wavefunction, Inc.[47] for the iron(III) complexes of $H_3L_N{}^{236}$, $H_3L_R{}^{236}$, $H_3L_N{}^{234}$, and $H_3L_R{}^{234}$ using methodology described in the Supporting Information.[48]

Growth Promotion Assays. The biological activity of $H_3L_N{}^{236}$ was studied using growth promotion bioassays of wild-type and mutant Gram-positive and Gram-negative bacteria using methods described previously[49,50] and that are found in the Supporting Information.[48]

Results

Ligand pK_a's. $H_3L_N{}^{236}$ (Figure 1) easily dissolves in 0.1 M $NaClO_4$, and all three hydroxamic acid deprotonation

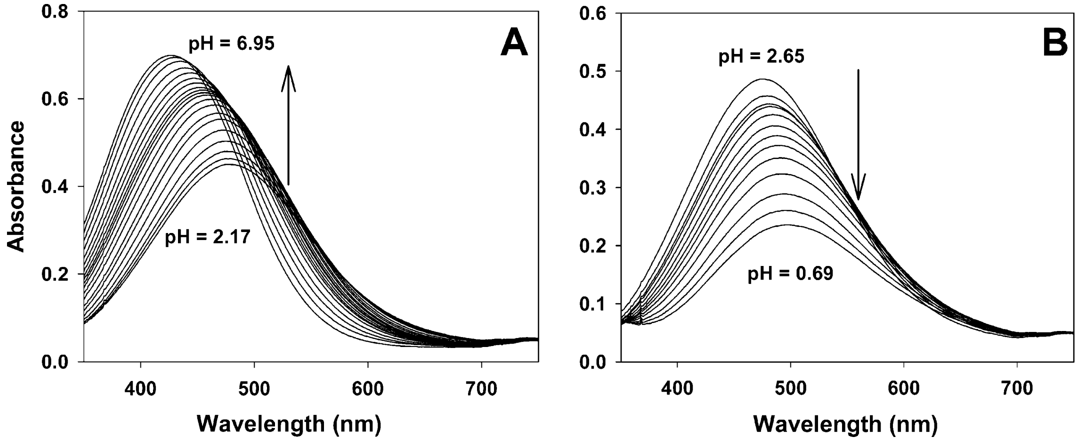

Figure 3. UV−vis spectra of $Fe^{III}-H_3L_N^{236}$ as a function of pH: (A) From pH 2.17 to 6.95; (B) From pH 2.65 to 0.69. Conditions: $H_3L_N^{236}$ and Fe^{3+}, 1:1, 2.5×10^{-4} M; $T = 298$ K; and $\mu = 0.10$ M $NaClO_4$.

constants were determined by the potentiometric titration of an acidified solution. The potentiometric equilibrium profiles for free $H_3L_N^{236}$ and its Fe(III) complex are shown in Figure 2. The deprotonation constants, K_{an} ($n = 1$, 2, and 3), for $H_3L_N^{236}$ are defined by eqs 1 and 2, and the values obtained from the refinement of potentiometric data are listed in Table 1 as pK_{an} ($-\log(K_{an})$).

$$H_{4-n}(L_N^{236})^{+1-n} \underset{}{\overset{K_{an}}{\rightleftharpoons}} H_{3-n}(L_N^{236})^{0-n} + H^+ \tag{1}$$

$$K_{an} = \frac{[H_{3-n}(L_N^{236})^{0-n}][H^+]}{[H_{4-n}(L_N^{236})^{+1-n}]} \tag{2}$$

The three acid dissociation constants determined for $H_3L_N^{236}$ fall in the normal range (pK_a = 8−10) for hydroxamic acids,[51−53] and successive values differ by 0.68 and 0.44 log units. The first difference is slightly greater than the expected statistical factor (0.48 log units),[54] suggesting a small degree of intramolecular interaction between the hydroxamate groups. This was also observed for the retrohydroxamate $H_3L_R^{234}$ (Figure 1) where the differences in successive deprotonation constants are 0.64 and 0.63 log units (Table 1). All three pK_a values for the deprotonation of $H_3L_N^{236}$ are slightly higher than the retrohydroxamate, $H_3L_R^{234}$ (Figure 1) and are consistently higher than other natural trihydroxamate siderophores (Table 1).[55,56]

Fe(III) Complex Formation and Protonation Equilibria. General Considerations. The potentiometric titration curve for $H_3L_N^{236}$ in the presence of an equivalent concentration of Fe(III) is shown in Figure 2. This mid-pH range titration curve exhibits a large jump at $a = 3$, indicative of easy release of three protons from the hydroxamate groups upon Fe(III) binding. This gives rise to a buffer region in the lower part of the titration curve, while the steep inflection at $a = 3$ represents the tight binding of Fe(III). This buffer region signifies that the pK_a's of the liberated three protons lie well below pH 4. In the low-pH range of the potentiometric titration, the free H^+ concentration is much larger compared to the concentration of metal, ligand, and the protons released due to metal chelation. Therefore, the low-pH potentiometric data are complemented with the spectrophotometric data for a more accurate description of the complexation equilibria.

Strong ligand-to-metal charge transfer (LMCT) bands characteristic of a Fe(III)−hydroxamate complex serve as the spectroscopic handle for monitoring the titrations of the $Fe^{III}-H_3L_N^{236}$ complex. Spectrophotometric titrations of $H_3L_N^{236}$ in the presence of an equivalent concentration of Fe(III) were carried out over two distinct pH regimes: mid-pH range (pH > 2.1), Figure 3A, and low-pH range (pH < 2.6), Figure 3B. This was necessary because of the two distinct electrode calibration methods used for mid- and low-pH range. Together, the mid- and low-pH experiments account for all the $Fe^{III}-H_3L_N^{236}$ species and their corresponding multiple equilibria in solution. The mid-range spectrophotometric experiments primarily include the equilibrium between fully chelated $Fe^{III}-H_3L_N^{236}$ complex and its singly protonated form, while the presence of some doubly protonated form of the complex is also observed at the low-pH end of these series. The titration is carried out separately and in both directions, from pH 2 to 7 and from pH 7 to 2, with no loss in the intensity of the LMCT bands, indicative of complete reversibility in the Fe(III) sequestration process and no significant ligand hydrolysis over the experimental pH range. Above pH 9, the LMCT band shows a very slow loss in intensity, which is attributed to ligand hydrolysis. The low-pH experiments (Figure 3B) are crucial, as they include the equilibrium between singly and doubly protonated forms of the $Fe^{III}-H_3L_N^{236}$ complex. Finally, at very low pH, one observes a loss in the intensity of the LMCT band resulting

---

(49) Schumann, G.; Möllmann, U. *Antimicrob. Agents Chemother.* **2001**, *45*, 1317−1322.
(50) Schumann, G.; Möllmann, U.; Heinemann, I. Patent application DE 19817021,9. (April 17, 1998).
(51) Monzyk, B.; Crumbliss, A. L. *J. Org. Chem.* **1980**, *45*, 4670−4675.
(52) Brink, C. P.; Fish, L. L.; Crumbliss, A. L. *J. Org. Chem.* **1985**, *50*, 2277−2281.
(53) Brink, C. P.; Crumbliss, A. L. *J. Org. Chem.* **1982**, *47*, 1171−1176.
(54) Noszal, B. *Biocoordination Chemistry: Coordination Equilibria in Biologically Active Systems*; Burger, K., Ed.; Ellis Horwood: New York, 1990; pp 18−55.
(55) Anderegg, G.; L'Eplattenier, F.; Schwarzenbach, G. *Helv. Chim. Acta* **1963**, *46*, 1409−1422.
(56) Wong, G. B.; Kappel, M. J.; Raymond, K. N.; Matzanke, B.; Winkelmann, G. *J. Am. Chem. Soc.* **1983**, *105*, 810−815.

Scheme 1. Counter-Clockwise from Bottom Left to Top Illustrates the Stepwise Chelation of $\mathrm{Fe_{aq}}^{3+}$ by $\mathrm{H_3L_N}^{236}$ Showing Equilibrium Constants (pK_n) and Number of Coordinated Hydroxamate Groups for Each Step. Clockwise from Top Left Illustrates H^+-Driven Dissociation of Pendant Arms Starting with the 2-Position; See Text.

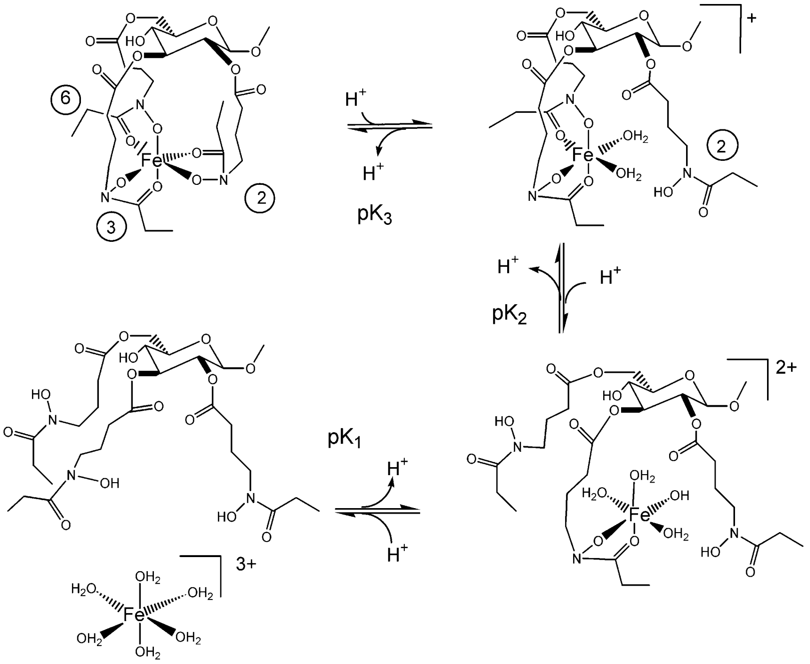

from a complete protonation of the $\mathrm{Fe^{III}}-\mathrm{H_3L_N}^{236}$ complex and the dissociation of $\mathrm{Fe_{aq}}^{3+}$.

$\mathrm{Fe^{III}}-\mathrm{H_3L_N}^{236}$ Complex Equilibria. The characteristic LMCT band of the Fe(III)−hydroxamate complex allows the proton-dependent $\mathrm{Fe^{III}}-\mathrm{H_3L_N}^{236}$ complexation equilibria to be studied spectrophotometrically. The spectrophotometric titrations of the $\mathrm{Fe^{III}}-\mathrm{H_3L_N}^{236}$ complex over two different pH regimes is illustrated in Figure 3. During these titrations from pH 0.6 to 7, three different spectroscopically distinguishable forms of the $\mathrm{Fe^{III}}-\mathrm{H_3L_N}^{236}$ complex are identified. At the low-pH end of the titration, the LMCT band displays a $\lambda_{\max}$ at 505 nm ($\epsilon = 1120$ $\mathrm{M^{-1}\ cm^{-1}}$), characteristic of a mono(hydroxamato)−Fe(III) complex.[5] The presence of this characteristic LMCT band at a pH as low as 0.6 suggests that $\mathrm{H_3L_N}^{236}$ is capable of complexing $\mathrm{Fe_{aq}}^{3+}$ at a very low pH. With a gradual rise in pH to 2 and above, the absorption maximum of the LMCT band shifts from 505 to 473 nm ($\epsilon = 2335$ $\mathrm{M^{-1}\ cm^{-1}}$), characteristic of the formation of a bis(hydroxamato)−Fe(III) complex.[5] Further increases in the pH to 7 and above gives rise to a third form of $\mathrm{Fe^{III}}-\mathrm{H_3L_N}^{236}$ species with $\lambda_{\max} = 428$ nm ($\epsilon = 2950$ $\mathrm{M^{-1}\ cm^{-1}}$). This is characteristic of a tris(hydroxamato)−Fe(III) complex. Thus, at pH 7 and above $\mathrm{H_3L_N}^{236}$ fully occupies all six coordination sites on Fe(III) using its three hydroxamate groups. This structural characterization of the $\mathrm{Fe^{III}}-\mathrm{H_3L_N}^{236}$ complex, involving the coordination of Fe(III) by three hydroxamate groups, is consistent with that seen for other natural and synthetic trihydroxamate siderophores.[5]

The spectrophotometric data were analyzed using the programs SPECFIT[45] and HYPERQUAD[44] to obtain three pK_a values listed in Table 2 for the $\mathrm{Fe^{III}}-\mathrm{H_3L_N}^{236}$ system, corresponding to the equilibrium between the mono-, bis-, and tris-complexes. These two data refinement methods yield values in excellent agreement within experimental error. Complementary analysis of potentiometric and spectrophotometric data provides a detailed and more accurate picture of the Fe(III) complexation process by $\mathrm{H_3L_N}^{236}$ and the nature of proton dissociation events taking place at the first coordination shell of Fe(III). These proton dissociation events for $\mathrm{Fe^{III}}-\mathrm{H_3L_N}^{236}$ are summarized in a generalized form by the stepwise equilibria shown in eqs 3−4 ($n = 1$, 2, and 3); the water molecules involved in the equilibria are omitted for simplicity and p$K_n = -\log \mathrm{K}_n$.

$$\{\mathrm{Fe^{III}}-\mathrm{H}_{4-n}\mathrm{L_N}^{236}\}^{+4-n} \xrightleftharpoons{K_{\mathrm{Fe(III)H}_{4-n}\mathrm{L_N}^{236}}} \{\mathrm{Fe^{III}}-\mathrm{H}_{3-n}\mathrm{L_N}^{236}\}^{+3-n} + \mathrm{H}^+ \qquad (3)$$

$$K_n = \frac{[\{\mathrm{Fe^{III}}-\mathrm{H}_{3-n}\mathrm{L_N}^{236}\}^{+3-n}][\mathrm{H}^+]}{[\{\mathrm{Fe^{III}}-\mathrm{H}_{4-n}\mathrm{L_N}^{236}\}^{+4-n}]} \qquad (4)$$

Spectrophotometric titration data along with the calculated pK_a values provide a complete picture of the Fe(III) chelation equilibria. The trihydroxamic acid $\mathrm{H_3L_N}^{236}$ starts to coordinate to Fe(III) at a very low pH. At pH 0.6, one hydroxamate group is already coordinated to Fe(III). The first pK_a, pK_1, of the $\mathrm{Fe^{III}}-\mathrm{H_3L_N}^{236}$ complex was calculated to be 0.66 and 0.88 using SPECFIT and HYPERQUAD, respectively; these values obtained from two different data refinement techniques are consistent within experimental error. The pK_1 is assigned to the proton release from $\mathrm{H_3L_N}^{236}$ when it initiates the Fe(III) complexation process (Scheme 1). The second acid dissociation at the first coordination shell involves the release of a proton from a second hydroxamic acid group as complexation proceeds from a mono(hydroxamato)tetraa-

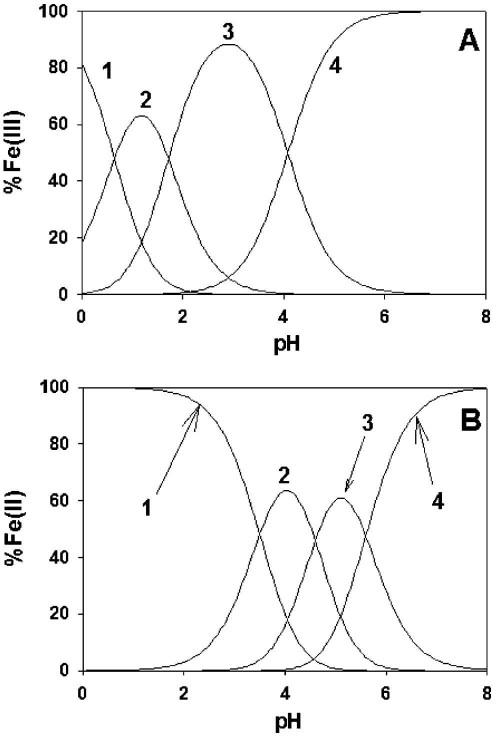

Figure 4. Calculated species distribution for (A) Fe(III) and (B) Fe(II) complexes of $H_3L_N^{236}$. Metal-containing species are normalized to the total concentration of iron. Legend: (A) 1 = Fe_{aq}^{3+} + $H_3L_N^{236}$, 2 = $Fe^{III}(H_2L_N^{236})(OH_2)_4^{2+}$, 3 = $Fe^{III}(HL_N^{236})(OH_2)_2^{+}$, 4 = $Fe^{III}(L_N^{236})$. (B) 1 = Fe_{aq}^{2+} + $H_3L_N^{236}$, 2 = $Fe^{II}(H_2L_N^{236})(OH_2)_4^{+}$, 3 = $Fe^{II}(HL_N^{236})(OH_2)_2$, 4 = $Fe^{II}(L_N^{236})^{-}$. Conditions: $H_3L_N^{236}$ + Fe^{3+} (Fe^{2+}), 1:1; T = 298 K; and μ = 0.10 M $NaClO_4$.

quo−Fe(III) complex to a bis(hydroxamato)diaquo−Fe(III) complex (Scheme 1). Nearly identical pK_2 values of 1.71 and 1.72 were determined from the two different data refinement techniques for the second acid dissociation step. Last, the two different data analysis techniques determined pK_3 to be 4.06 and 4.08, which are identical within experimental error. This pK_3 is assigned to the proton dissociation as complexation proceeds from a bis(hydroxamato)diaquo−Fe(III) to a tris(hydroxamato)−Fe(III) complex, a fully coordinated $Fe^{III}(L_N^{236})$ complex (Scheme 1).

The potentiometric and spectrophotometric results for the $Fe^{III}-H_3L_N^{236}$ complex protonation equilibria are summarized in Scheme 1. Strain energy calculations (see Supporting Information for details)[48] were conducted for the gas phase which suggest that protonation and release of the 2-position pendant arm hydroxamate moiety occurs first from $Fe^{III}(L_N^{236})$, as shown in Scheme 1 (Table S3). The subsequent order of arm protonation and release cannot be discerned from our calculations. A species distribution plot (Figure 4A) generated from the pK_n values for the $Fe^{III}-H_3L_N^{236}$ complex clearly shows the tris(hydroxamato)−Fe(III) complex $Fe^{III}(L_N^{236})$ as the predominant species above pH 5. Thus the fully sequestered iron(III) complex without a net charge is the only species present at neutral pH and above.

The overall stability (i.e., the usual proton independent stability constant found in compilations of metal−ligand stability constants[46]) of the Fe(III) complex of $H_3L_N^{236}$ (log $\beta^{III}{}_{110}$) can be defined by eqs 5 and 6.

$$Fe_{aq}{}^{3+} + [L_N{}^{236}]^{3-} \rightleftharpoons Fe^{III}(L_N{}^{236}) \tag{5}$$

$$\beta^{III}{}_{110} = \frac{[Fe^{III}(L_N{}^{236})]}{[Fe_{aq}{}^{3+}][(L_N{}^{236})^{3-}]} \tag{6}$$

The log $\beta^{III}{}_{110}$ value for the $Fe^{III}-H_3L_N^{236}$ equilibrium system investigated here (and for most other Fe(III)−siderophore systems) must be indirectly calculated, since at pH values high enough to produce the fully deprotonated chelator, $[L_N^{236}]^{3-}$, Fe_{aq}^{3+} will hydrolyze and precipitate. Two methods were used in our study to indirectly calculate log $\beta^{III}{}_{110}$ described in eqs 5 and 6.

In the first method, a series of competition experiments with EDTA were carried out at various pH values. The competition equilibrium is summarized in eqs 7 and 8.

$$Fe^{III}(L_N{}^{236}) + EDTA \overset{K}{\rightleftharpoons} Fe^{III}EDTA + L_N{}^{236} \tag{7}$$

$$K = \frac{[Fe^{III}EDTA][(L_N{}^{236})]}{[Fe^{III}(L_N{}^{236})][EDTA]} = \frac{\beta^{FeEDTA}}{\beta^{III}} \tag{8}$$

The water molecules and molecular charges involved in the equilibrium are omitted for clarity. The concentrations of $Fe^{III}(L_N^{236})$ were calculated from the absorbance at 428 nm, where $Fe^{III}(L_N^{236})$ is the only light-absorbing species. These data were used to obtain the overall Fe(III)-binding constant for $[L_N^{236}]^{3-}$ using literature data for $\beta^{III}{}_{110}$ for FeEDTA[46] and SPECFIT software.[45] A model involving two ligands and a metal were used to refine the spectrophotometric competition data, and a stability constant, log $\beta^{III}{}_{110}$, corresponding to eq 5 was calculated to be 31.1 (Table 3).

In a second method, the potentiometric and the spectrophotometric titration data were used to calculate the overall stability constant, log $\beta^{III}{}_{110}$, for $Fe^{III}(L_N^{236})$ as described in eqs 5 and 6. These data were analyzed independently using the software HYPERQUAD[44] and SPECFIT,[45] and the calculated log $\beta^{III}{}_{110}$ values are listed in Table 3. The log $\beta^{III}{}_{110}$ values calculated from these two different methods of data analysis are in excellent agreement with each other and are within experimental error of the value obtained by EDTA competition. These results are comparable to those observed for trihydroxamic-acid-based natural siderophores and siderophore analogues (Table 3).[36,55−59]

The pFe value (−log[Fe_{aq}^{3+}] at pH 7.4 with a total ligand concentration of 10^{-5} M and total Fe(III) concentration of 10^{-6} M)[60] for $H_3L_N^{236}$ was calculated to be 26.1. The pFe value is used to compare the Fe(III) chelating properties of $H_3L_N^{236}$ with other Fe(III) chelators at physiological conditions. A pFe of 26.1 calculated for $H_3L_N^{236}$ is slightly better than observed for desferrichrome and slightly lower than the value calculated for the retrohydroxamate $H_3L_R^{234}$ (Table 3).

Fe(III)/Fe(II) Redox and Fe(II) Chelation. A quasi-reversible cyclic voltammogram was obtained for the

---

(57) Schwarzenbach, G.; Schwarzenbach, K. *Helv. Chim. Acta* **1963**, *46*, 1390−1400.

(58) Loomis, L. D.; Raymond, K. N. *Inorg. Chem.* **1991**, *30*, 906−911.

(59) Albrecht-Gary, A.-M.; Blanc, S.; Rochel, N.; Ocaktan, A. Z.; Abdallah, M. A. *Inorg. Chem.* **1994**, *33*, 6391−6402.

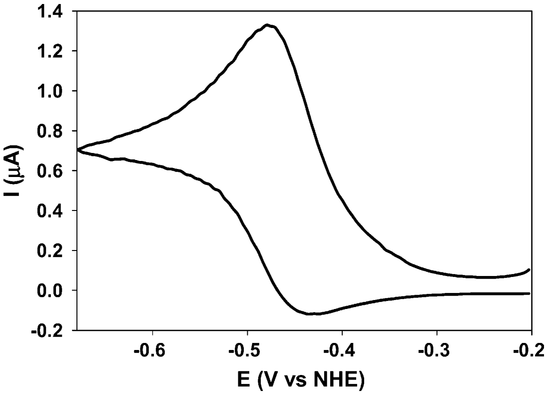

Figure 5. Cyclic voltammogram of $Fe^{III}(L_N^{236})$. Conditions: [Fe] = 1 × 10^{-3} M, $[H_3L_N^{236}]$ = 1 × 10^{-2} M, pH 9.1. HDME working electrode, scan rate = 20 mV/s, T = 298 K, and μ = 0.10 M ($NaClO_4$). $E_{1/2}$ = −454 mV with a peak separation of 90 mV.

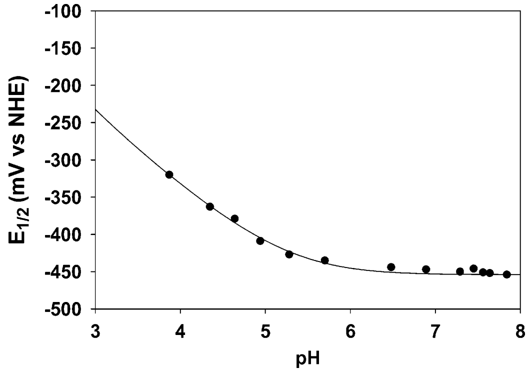

Figure 6. $Fe^{III}(L_N^{236})$ reduction potential ($E_{1/2}$) as a function of pH. Conditions: [Fe] = 1 × 10^{-3} M, $[H_3L_N^{236}]$ = 1 × 10^{-2} M. HDME working electrode, scan rate = 20 mV/s, T = 298 K, and μ = 0.10 M ($NaClO_4$). The solid circles represent data points used in the nonlinear regression analysis. The solid line represents a plot of eq 13 where E_{aquo} = +732 mV, $\beta^{III}{}_{110} = 10^{31.16}$, $\beta^{II}{}_{110} = 10^{10.5}$, $K_{Fe(III)HL_N{}^{236}} = 10^{4.08}$ and $K_{Fe(II)HL_N{}^{236}}$, $K_{Fe(II)H_2L_N{}^{236}}$ and $K_{Fe(II)H_3L_N{}^{236}}$ were determined by nonlinear least-square analysis to be$10^{5.6}$, $10^{4.6}$, and $10^{3.5}$, respectively.

$Fe^{III}(L_N^{236})$ complex at pH 9.1 (Figure 5) with a half-wave potential ($E_{1/2}$) of −454 mV (vs NHE), corresponding to the Fe(III)/Fe(II) couple. The significantly negative reduction potential for the Fe(III)/Fe(II) couple is indicative of the ligand's greater selectivity for Fe(III) over Fe(II).[4] This selectivity is directly reflected in the stability constant for Fe(III) and Fe(II) complexes of $H_3L_N^{236}$, as described by a modified form of the Nernst equation, eq 9

$$E_{aquo} - E_{complex} = 59.15 \log(\beta^{III}{}_{110}/\beta^{II}{}_{110}) \qquad (9)$$

where $\beta^{III}{}_{110}$ and $\beta^{II}{}_{110}$ represent the overall stability constant for $Fe^{III}(L_N^{236})$ and $Fe^{II}(L_N^{236})^-$, respectively. Equation 9 along with the $\beta^{III}{}_{110}$ value determined above and the E_{aquo} value for the $Fe(H_2O)_6{}^{3+}/Fe(H_2O)_6{}^{2+}$ couple allows for the calculation of a $\beta^{II}{}_{110}$ value for the overall stability of the $Fe^{II}(L_N^{236})^-$ complex (Table 3).

The cyclic voltammogram shows very little change in $E_{1/2}$ for the Fe(III)/Fe(II) couple and remains quasi-reversible in the pH range 7−9. Below this pH range, the anodic and cathodic peaks broaden as the estimated $E_{1/2}$ shifts to more positive values. This strong pH dependence of the observed $E_{1/2}$ (Figure 6) is attributed to the protonation and dissociation of the hydroxamate groups in the Fe(III) and Fe(II) complex following reduction, as represented by eqs 3 and 10−12, over the experimental pH range.

$$Fe^{III}(L_N{}^{236}) + e^- \rightleftharpoons Fe^{II}(L_N{}^{236})^- \qquad (10)$$

$$\{Fe^{II}-H_{4-n}L_N{}^{236}\}^{+3-n} \xrightleftharpoons{K_{Fe(II)H_{4-n}L_N{}^{236}}} \{Fe^{II}-H_{3-n}L_N{}^{236}\}^{+2-n} + H^+ \qquad (11)$$

$$K_n = \frac{[\{Fe^{II}-H_{3-n}L_N{}^{236}\}^{+2-n}][H^+]}{[\{Fe^{II}-H_{4-n}L_N{}^{236}\}^{+3-n}]} \qquad (12)$$

The pH dependence of the reduction potential profile in Figure 6 was analyzed using an equilibrium model that includes four distinct single-protonation reactions, three protonation reactions for three different Fe(II) complexes and a single protonation of the $Fe^{III}(L_N^{236})$ complex, as determined from the speciation diagram shown in Figure 4A. For such a system, the observed formal reduction potential should vary as

$$\begin{aligned} E_f = E_{aquo} - 59.15 \log\left\{\frac{\beta^{III}{}_{110}}{\beta^{II}{}_{110}}\right\} + \\ 59.15 \log(1 + K_{Fe(II)HL_N{}^{236}}[H^+] + \\ K_{Fe(II)HL_N{}^{236}}K_{Fe(II)H_2L_N{}^{236}}[H^+]^2 + \\ K_{Fe(II)HL_N{}^{236}}K_{Fe(II)H_2L_N{}^{236}}K_{Fe(II)H_3L_N{}^{236}}[H^+]^3) - \\ 59.15 \log(1 + K_{Fe(III)HL_N{}^{236}}[H^+]) \qquad (13) \end{aligned}$$

where E_{aquo} is the standard reduction potential of the $Fe(H_2O)_6{}^{3+}/Fe(H_2O)_6{}^{2+}$ couple, $\beta^{III}{}_{110}$ and $\beta^{II}{}_{110}$ are the overall stability constants for the Fe(III) and Fe(II) hexacoordinated complexes, respectively, $K_{Fe(II)H_nL_N{}^{236}}$ are the stepwise protonation constants of the Fe(II) complex, and $K_{Fe(III)HL_N{}^{236}}$ is the first protonation constant of the Fe(III) complex. During a nonlinear least-squares refinement of the data shown in Figure 6 using eq 13, the value of $K_{Fe(III)HL_N{}^{236}}$ was fixed at $10^{4.08}$ (the value obtained from the spectrophotometric titration). The Fe(II) complex protonation constants obtained from the nonlinear least-squares refinement are listed in Table 2. When the data were also analyzed using eq 13 and treating all of the protonation constants ($Fe^{III}(L_N^{236})$ and $Fe^{II}(L_N^{236})^-$) as variables, values for $K_{Fe(II)H_nL_N{}^{236}}$ were found to be identical with those listed in Table 2, and the computed value for $K_{Fe(III)L_N{}^{236}}$ was $10^{4.1}$. This is in excellent agreement with the value determined by spectrophotometric titration (Table 2) and supports the validity of the model used for the pH-dependent electrochemical data analysis. The Fe(II) complex protonation constants were used to generate a $Fe^{II}-H_3L_N^{236}$ speciation profile as a function of pH (Figure 4B).

---

(60) Raymond, K. N.; Müller, G.; Matzanke, B. F. *Top. Curr. Chem.*, Boschke, F. L., Ed.; Springer-Verlag: Berlin, Heidelberg, 1984; Vol. 123, pp 49−102.

Scheme 2. Fe(III)/Fe(II) Reduction Leads to a Loss of Iron Binding Affinity and Increased Protonation Susceptibility for $FeH_3L_N^{236}$ Complexes. Color Shading Denotes Identical pH Regimes (4, 2, 1) for the Fe(III) and Fe(II) Complexes, Which Emphasizes the Increased Ease of Protonation of the Reduced Form of the Complex.

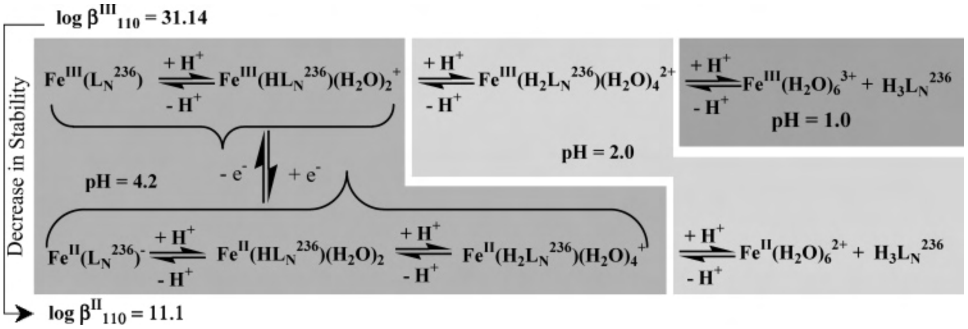

Biological Activity. The biological activity of $H_3L_N^{236}$ was studied in comparison to $H_3L_R^{234}$ using growth promotion bioassays of Gram-positive and Gram-negative bacteria including *Mycobacterium smegmatis*, *Pseudomonas aeruginosa*, *Salmonella typhimurium*, and *Escherichia coli* comprising wild-type strains and also including siderophore biosynthesis, siderophore receptor, and general iron transport mutants. The details of these growth promotion results are reported in the Supporting Information.[48]

Both $H_3L_N^{236}$ and $H_3L_R^{234}$ promoted the growth of the wild-type and the mutant strains of *P. aeruginosa*, as well as the *S. typhimurium* mutant, based on growth spot diameter in comparison with the standard siderophore ferricrocin (Table S7). This suggests that our observed siderophore activity does not depend on ligand exchange with the natural siderophores pyoverdin, pyochelin, or enterobactin and is independent of the presence of the pyoverdin receptor. While active, $H_3L_N^{236}$ was somewhat less active than $H_3L_R^{234}$ in all cases.

Consistent with previous results,[49] both $H_3L_N^{236}$ and $H_3L_R^{234}$ in the iron-loaded ferri-forms act as significant growth promotors for *M. smegmatis* and are independent of the mycobacterial exochelin/mycobactin uptake route (Table S8). In contrast, growth-promoting activity of ferricrocin depends on ligand exchange with either mycobactin or exochelin. It does not promote growth of the exochelin/mycobactin biosynthesis deletion mutant and the mycobactin biosynthesis exochelin permease (uptake) deletion mutant. $H_3L_R^{234}$ exhibits slight activity as the desferri compound, whereas $H_3L_N^{236}$ does not, again suggesting the somewhat higher growth-promotion activity of the former (Table S8).

For *E. coli*, $H_3L_N^{236}$ was not active at all in contrast to the excellent activity of $H_3L_R^{234}$, indicating possible subtle effects related to molecular recognition (Table S9). Also, as expected, $H_3L_R^{234}$ did not exhibit siderophore activity for the *E. coli* TonB mutant strain in which all siderophore iron transport systems are switched off. This demonstrates an active uptake mechanism for the $Fe^{III}(L_R^{234})$ complex. This uptake depends primarily on the ferrichrome receptor FhuA, but to a lesser degree, it also depends on the coprogen, ferrioxamine B and rhodotorulic acid receptor FhuE, as demonstrated by the extinguished or reduced siderophore activity for the relevant deletion mutant strains (Table S9).

Discussion

The synthetic desferrichrome mimic, $H_3L_N^{236}$, sequesters Fe(III) with a very high overall stability similar to that of desferrichrome and desferrichrome analogues (Table 3), which makes $H_3L_N^{236}$ a thermodynamically attractive model for desferrichrome. The proton-dependent equilibrium studies indicate that the $Fe^{III}-H_3L_N^{236}$ complex undergoes three successive protonations corresponding to well-separated dechelation equilibria to form tris-, bis-, and monohydroxamato−Fe(III) complexes, as illustrated in Scheme 1 and the speciation plot in Figure 4. At physiological pH 7.4, $H_3L_N^{236}$ completely sequesters Fe_{aq}^{3+} as $Fe^{III}(L_N^{236})$ with a pFe $=$ 26.1. This is in the upper range observed for trihydroxamate systems, both natural and synthetic, but slightly lower than that of the structural isomer $H_3L_R^{234}$ (Figure 1). It has previously been noted that a retro-hydroxamate isomer sequesters Fe(III) slightly more tightly than the normal isomer.[61,62] The high pFe of $H_3L_N^{236}$ suggests that $H_3L_N^{236}$ has a thermodynamic advantage over transferrin for Fe(III) chelation. This thermodynamic advantage can be potentially used in designing the next generation of iron-overload drugs.

A very negative redox potential for the $Fe^{III}(L_N^{236})/Fe^{II}(L_N^{236})^-$ couple emphasizes the high stability and selectivity of $H_3L_N^{236}$ for Fe(III). These redox results also demonstrate that complex stability is dramatically decreased on reduction to Fe(II) ($\beta^{III}_{110} = 10^{31.14}$; $\beta^{II}_{110} = 10^{11.1}$), thereby facilitating the release of iron by lowering the thermodynamic barrier. Additionally, the kinetic lability of the reduced complex is highly enhanced and the susceptibility of $Fe^{II}(L_N^{236})^-$ toward protonation is dramatically increased (Scheme 2 and Figure 4). Therefore, reduction of the Fe(III) complex to an Fe(II) complex with subsequent protonation can provide a pathway for overcoming the very high thermodynamic stability of Fe(III)−siderophore complexes and provide for a facile release of iron and delivery to the cell.

The two saccharide trihydroxamic acids, $H_3L_N^{236}$ and $H_3L_R^{234}$ (Figure 1), have two significant structural variations: the point of attachment of the three arms to the saccharide backbone and the orientation of the iron binding

---

(61) Motekaitis, R. J.; Sun, Y.; Martell, A. E. *Inorg. Chem.* **1991**, *30*, 1554−1556.

(62) Nguyen-van-Duong, M. K.; Guillot, V.; Nicolas, L.; Gaudemer, A.; Lowry, L.; Spasojevic, I.; Crumbliss, A. L. *Inorg. Chem.* **2001**, *40*, 5948−5953.

hydroxamate moieties at the end of each arm (normal hydroxamate and retrohydroxamate). Despite these structural differences, a relatively small variation was observed with respect to the iron binding properties of these ligands (Tables 1, 2, and 3), suggesting that the solution chelation chemistry is not very sensitive to these structural changes. However, strain energy calculations suggest that the two structural variations may have opposing effects. Strain energy calculations (Supporting Information, Table S1)[48] for the gas phase demonstrate that $[L_N^{236}]^{3-}$ and $[L_R^{234}]^{3-}$ show comparable strain upon sequestration of Fe(III), with a 40 kcal/mol (20%) greater strain calculated for $Fe^{III}(L_N^{236})$, which is qualitatively consistent with our observed slightly lower β^{III}_{110} value. Strain energy calculations for all structural permutations (H_3L^{234} and H_3L^{236} pendant arm isomers and H_3L_R and H_3L_N retro and normal hydroxamate binding group isomers) suggest that the retro isomer exhibits less strain and that the effect is greater with {234} arm positions over {236}. However, variation in the arm position produces variable results with {234} showing less strain for the retro isomer and more strain for the normal isomer. This suggests that the modest difference in β^{III}_{110} values for $Fe^{III}(L_N^{236})$ and $Fe^{III}(L_R^{234})$ are due to opposing effects on the strain energy, with the disadvantage of the normal hydroxamate moiety configuration being counterbalanced by a more favorable pendant arm position in $Fe^{III}(L_N^{236})$ relative to $Fe^{III}(L_R^{234})$. Strain energy calculations also suggest that initial protonation and hydroxamate moiety dissociation occurs at the 2-position arm (Scheme 1, Table S3). Initial release of the pendant arm in the 4-position is predicted for $Fe^{III}(L_R^{234})$ (Table S3).

Both $H_3L_N^{236}$ and $H_3L_R^{234}$ were shown to be biologically active through growth promotion bioassays. While the generally higher siderophore activity of $H_3L_R^{234}$ may be due to the slightly stronger Fe(III) binding and the more facile protonation of the complex in both the Fe(III) and Fe(II) forms to produce the more open and labile diaquo complexes ($Fe^{III}(HL_R^{234})(OH_2)_2^+$ and $Fe^{II}(HL_R^{234})(OH_2)_2$),[63] the difference in siderophore activity may also be due to the influence of the structural features related to the receptor recognition of the siderophore Fe(III) complex. The biological and the thermodynamic data together suggest that $H_3L_N^{236}$ and $H_3L_R^{234}$ can both function as siderophore mimics.

Strong thermodynamics of Fe(III) chelation and promising growth promotion from biological studies are clear indications of the saccharide backbone's suitability as a platform for siderophore design. Along with the structural features that favor receptor recognition and cellular uptake, the saccharide backbone enhances the aqueous solubility of the ligand, which is sometimes lacking among other synthetic analogues. The connecting points and the orientation of the metal-chelating hydroxamate groups appear to have only a small influence on the overall Fe(III) chelation properties of these ligands. The saccharide-based hydroxamate siderophore analogues, $H_3L_N^{236}$ and $H_3L_R^{234}$, thermodynamically and biologically satisfy the requirements for an effective siderophore mimic. These findings will serve as the basis for future rational design and synthesis of siderophore analogues to explore the specifics of structure−function relationships during Fe(III) chelation and receptor recognition processes.

Summary and Conclusions

The aqueous Fe(III) coordination chemistry of a ferrichrome analogue, 1-*O*-methyl-2,3,6-tris-*O*-[4-(*N*-hydroxy-*N*-ethylcarbamoyl)-*n*-butyryl]-α-D-glucopyranoside ($H_3L_N^{236}$), with a chiral saccharide platform was explored and compared to that of a structurally related retrohydroxamate, $H_3L_R^{234}$, synthesized on the identical saccharide platform. Though structurally different, the two saccharide-based ferrichrome analogues are similar in their overall Fe(III) coordination properties. The thermodynamic and the spectroscopic properties of $H_3L_N^{236}$ closely parallel those of Fe[ferrichrome] and previously characterized ferrichrome analogues, while the Fe(III) binding affinity is superior, based on β^{III}_{110} and pFe values. The very high pFe for $H_3L_N^{236}$ indicates it has the ability to be an effective chelating agent at physiological conditions and suggests that from a strictly thermodynamic standpoint it is possible for $H_3L_N^{236}$ to remove Fe(III) from transferrin, a favorable characteristic for application as an iron-overload drug. Thermodynamic and biological data reported here imply that these ferrichrome analogues with a saccharide platform are excellent siderophore mimics and attractive substrates for cell receptor proteins. A comparative thermodynamic investigation of the ferric and ferrous complexes ($Fe^{III}(L_N^{236})$ and $Fe^{II}(L_N^{236})^-$) and their corresponding protonation constants demonstrates that redox-coupled protonation is an attractive mechanism for iron release from these very stable Fe−siderophore complexes during transport into the cell.

Acknowledgment. We thank Claire J. Parker Siburt for helpful discussions and the National Science Foundation (CHE-0079066 and CHE-0418006) for financial support.

Supporting Information Available: Glass electrode calibration methods, listings of computational simulation procedures and results, and growth promotion assay procedures and results. This material is available free of charge via the Internet at http://pubs.acs.org.

IC070158L

---

(63) Compare Figure 4 with Figure 4 in ref 36.

(64) Wawrousek, E. F.; McArdle, J. V. *J. Inorg. Biochem.* **1982**, *17*, 169−183.

(65) Bickel, H.; Hall, G. E.; Keller-Schierlein, W.; Prelog, V.; Vischer, E.; Wettstein, A. *Helv. Chim. Acta* **1960**, *43*, 2129−2138.

(66) Cooper, S. R.; McArdle, J. V.; Raymond, K. N. *Proc. Natl. Acad. Sci.* **1978**, *75*, 3551−3554.

(67) Spasojevic, I.; Armstrong, S. K.; Brickman, T. J.; Crumbliss, A. L. *Inorg. Chem.* **1999**, *38*, 449−454.